Applied Catalysis B: Environmental 237 (2018) 263–272

Contents lists available at ScienceDirect

Applied Catalysis B: Environmental

journal homepage: www.elsevier.com/locate/apcatb

Local dynamics of copper active sites in zeolite catalysts for selective catalytic reduction of NO_x with NH_3

Peirong Chen[a,b,c,*], Abhishek Khetan[c,d], Magdalena Jabłońska[c,e], Johannes Simböck[c,e], Martin Muhler[f], Regina Palkovits[c,e], Heinz Pitsch[c,d], Ulrich Simon[b,c,*]

[a] Guangdong Provincial Key Laboratory of Atmospheric Environment and Pollution Control, School of Environment and Energy, South China University of Technology, 510006 Guangzhou, China
[b] Institute of Inorganic Chemistry, RWTH Aachen University, Landoltweg 1, 52074 Aachen, Germany
[c] Center for Automotive Catalytic Systems Aachen, RWTH Aachen University, Aachen, Germany
[d] Institute for Combustion Technology, RWTH Aachen University, Templergraben 64, 52056 Aachen, Germany
[e] Chair of Heterogeneous Catalysis and Chemical Technology, RWTH Aachen University, Worringerweg 2, 52074 Aachen, Germany
[f] Laboratory of Industrial Chemistry, Ruhr-University Bochum, 44780 Bochum, Germany

ARTICLE INFO

Keywords:
Impedance spectroscopy
DRIFTS
DFT calculation
Cu redox cycle
Modulus

ABSTRACT

In Cu-zeolite based selective catalytic reduction of NO_x with NH_3 (NH_3-SCR), Cu species (in particular Cu^I) solvated by NH_3 molecules are predicted theoretically to be highly mobile with their mobility being decisive for the NH_3-SCR reactivity at low temperatures (< 250 °C). Direct experimental observation of the Cu mobility after NH_3 solvation, however, has not been achieved yet. Here we show that complex impedance-based modulus spectroscopy, performed by following the corresponding dielectric relaxation processes at high frequencies (10^4 to 10^6 Hz), can be applied to monitor directly the dynamic local movement of Cu ions in zeolite catalysts under NH_3-SCR related reaction conditions. Simultaneous *in situ* impedance and infrared spectroscopy studies, assisted by periodic DFT calculations with reliable van der Waals dispersion corrections, allowed us to identify the key factors determining the local dynamics of Cu ions in two representative Cu-zeolites, *i.e.* Cu-ZSM-5 and Cu-SAPO-34. The co-adsorption and interaction of NO and NH_3 on Cu^{II} sites led to the formation of highly mobile Cu^I species and NH_4^+ intermediates, and, consequently, significantly enhanced local dynamics of Cu ions in both zeolite catalysts. The re-oxidation of Cu^I, which is the rate-determining step of NH_3-SCR reaction, was more favorable in Cu-SAPO-34 than in Cu-ZSM-5, which can be attributed to the close coupling of NH_4^+ intermediate and Cu site promoting the formation of Cu^{II}-NO_2/NH_4^+. As a result, the overall local dynamics of Cu, largely determined by Cu^I species, is less dependent on the NH_4^+ intermediate in Cu-SAPO-34 than in Cu-ZSM-5.

1. Introduction

Zeolites are widely used as host material to prepare highly dispersed transition-metal catalysts for redox reactions such as selective catalytic reduction (SCR) of nitrogen oxides (NO_x, x = 1, 2) [1–11], partial oxidation of methane to methanol [12–14], because of their unique physicochemical properties (*e.g.* porosity, acidity, stability, *etc.*). Under reaction conditions, the active metal sites located inside the zeolite framework structures often experience dynamic and reversible structural and/or electronic changes [2,12]. Unlike those irreversible modifications (*e.g.,* agglomeration of active sites, change of oxidation state) that can be detected *ex situ* after catalytic reactions [15–17], the reaction-driven or reaction-induced changes are usually only observable by *in situ* or *operando* methods [5,18,19]. One of the typical (and also extensively studied) examples is that of the isolated Cu sites in zeolite catalysts (including Cu^{II} which balances two framework Al centers, and $[Cu^{II}OH]^+$ that balances one framework Al center), which are solvated and mobilized by ammonia (NH_3) molecules in SCR reactions with NH_3 as the reducing agent (NH_3-SCR) [7–9,20]. By integrating density functional theory (DFT) computational models and experimental *operando* spectroscopy, Paolucci et al. and Lomachenko et al. unveiled that Cu species, regardless of the initial siting sites and the zeolite topology, are released from the equilibrium sites on the framework lattice and move rather freely within the zeolite cages or pores due to the NH_3 solvation effect at low temperatures (below 250 °C) [4,18]. Quantitative estimation of the mobility of Cu species by *ab initio* molecular dynamics (AIMD) simulations suggests that NH_3 solvation enhances the mobility of dehydrated Cu species at 298 K by a factor of 9.4 for Cu^{II}

* Corresponding authors.
E-mail addresses: chenpr@scut.edu.cn (P. Chen), ulrich.simon@ac.rwth-aachen.de (U. Simon).

https://doi.org/10.1016/j.apcatb.2018.05.091
Received 27 March 2018; Received in revised form 26 May 2018; Accepted 30 May 2018
Available online 31 May 2018
0926-3373/

and a factor of 15.8 for $[Cu^{II}OH]^+$, respectively [4]. Catalytic activity tests by different research groups revealed that the NH_3-solvated Cu species are responsible for the NH_3-SCR turnover (at 473 K), which is independent of the initial coordinating position and the zeolite framework type [4,6]. More recently, Paolucci et al. reported that NH_3-solvated Cu^I species, namely $Cu^I(NH_3)_2$, can travel between neighboring cages through the eight-member-ring (8MR) window in CHA zeolite to form transient Cu ion pairs participating in the O_2-mediated $Cu^I \rightarrow Cu^{II}$ re-oxidation, which is the rate-determining step in NH_3-SCR over Cu-CHA zeolite with low Cu density [2].

While the NH_3 solvation effect can be directly followed using combined X-ray absorption spectroscopy and X-ray emissions spectroscopy (XAS/XES), based on the change of the local coordination and preferential ligation of Cu species in zeolites [18,21], a direct observation of the constrained movement of Cu species has not been achieved experimentally yet. The movement of NH_3-solvated Cu species, either within a restricted volume close to the original equilibrium site in the zeolite lattice [4] or through the zeolite window to another cage [2,22], is expected to induce a change of dipole moment between the fixed charge of the polyanionic lattice and the positive charge of the mobile cations [23,24]. The subsequent dielectric relaxation of such rather local Cu movement can be probed by complex impedance spectroscopy (IS) and visualized in the corresponding spectral representation of the imaginary part of modulus *M*, *i.e.* M'' (so-called modulus spectroscopy). M'' is defined as

$$M'' = 2\pi f C_0 Z' \quad (1)$$

with *f* the perturbing frequency, C_0 the capacity of the empty capacitor, *i.e.* the geometric capacitance, and Z' the real part of the complex impedance *Z* (see *Supplementary Information* for more theoretical details of IS data presentation) [23,25].

Here, we report that complex impedance-based modulus spectroscopy enables to probe directly the local dynamics of NH_3-solvated Cu species in Cu-exchanged zeolites with different framework types (MFI and CHA) under carefully selected, SCR-related model reaction conditions. Specifically, we focused on Cu-ZSM-5 (MFI), which appears to be a highly interesting component for coupled SCR-NSR (NO_x storage reduction) systems [11,26], and Cu-SAPO-34 (CHA), a commercially relevant NH_3-SCR catalyst [27–29]. A series of Cu-ZSM-5 catalysts with low Cu exchange levels were carefully synthesized to ensure high dispersion of all the introduced Cu sites, and the local motion dynamics of the Cu sites in these Cu-ZSM-5 catalysts were systematically investigated. In order to identify the key factors determining the local dynamics of Cu ions in NH_3-SCR reactions, comparative investigations between Cu-ZSM-5 and Cu-SAPO-34 were carried out by means of modulus spectroscopy, simultaneous IS and diffuse reflectance infrared Fourier transform spectroscopy (IS-DRIFTS) studies under *in situ* conditions, and periodic DFT calculations using reliable van der Waals dispersion corrections from BEEF-vdW exchange-correlation functional [30,31].

2. Methodology

2.1. Sample synthesis and characterization

Cu-ZSM-5 zeolites were synthesized by aqueous ion exchange using commercially available H-ZSM-5 zeolite (Clariant) with a Si/Al ratio of 13.5 and following the protocol described elsewhere [32]. After ion exchange, the zeolite materials were filtered, thoroughly washed with distilled water (three times), and dried. The obtained powder samples were then calcined at 500 °C resulting in Cu-ZSM-5 catalysts. Increased Cu loading was achieved by repeating the ion exchange process before calcination. H-ZSM-5 which was used in comparative measurements was also calcined at 500 °C. Commercial Cu-SAPO-34 powders (Clariant) were calcined at 500 °C before any further use.

Actual Cu loadings in the Cu-ZSM-5 and Cu-SAPO-34 catalysts were analyzed using inductively coupled plasma optical emission spectroscopy (ICP-OES). Static N_2 physisorption measurements were carried out at −196 °C (77 K) using an Autosorb-1MP Quantachrome system. Samples were degassed at 200 °C for 2 h before the measurements. Specific surface area and porosity were determined based on the recorded adsorption isotherms. The crystal structures of all zeolite samples were analyzed by X-ray diffraction (XRD) using Cu Kα irradiation. Diffuse reflection ultraviolet/visible spectroscopy (DR UV–vis) measurements were performed in a Perkin-Elmer Lambda 650 UV–vis spectrophotometer equipped with a Praying Mantis (Harrick) mirror construction.

For temperature-programmed desorption of NH_3 as a probe molecule (NH_3-TPD), 50 mg of zeolite powders was loaded into a quartz U-tube reactor, and was first dried at 200 °C in flowing helium for 1 h before NH_3 dosing. The adsorption of NH_3 was carried out at 50 °C in flowing NH_3 atmosphere (4000 ppm NH_3 in helium) for 2 h. Afterwards, the reactor with zeolite catalyst was flushed with pure helium for 2 h to remove physically adsorbed NH_3. NH_3 desorption was performed in the temperature range from 50 °C to 650 °C at a ramping rate of 2 K min^{-1}. The outlet concentration of NH_3 was monitored downstream by a non-dispersive infrared detector (Emerson Process Management, Rosemount NGA 2000 MLT 4). The detector was calibrated with 4000 ppm NH_3 before each single measurement.

2.2. NH_3-SCR activity tests

Catalytic activities of the zeolite catalysts in NH_3-SCR were examined under atmospheric pressure in a fixed-bed micro-reactor (with an inner diameter of 6 mm and a length of 320 mm) [17,32]. The reactant concentrations were continuously monitored using a quadrupole mass spectrometer (QMS; MKS Cirrus 2) directly connected to the reactor outlet using a heated capillary. The gas mixture at the reactor inlet consisted of 2500 ppm NH_3, 2500 ppm NO, 2.5 vol. % O_2, and Ar balance (97.0 vol. %). The total flow rate of the reaction mixture was 40 ml min^{-1}. In each test, the catalyst (100 mg) was outgassed at 500 °C for 0.5 h in a flow of 5.0 vol. % O_2 diluted in Ar (20 ml min^{-1}), and NH_3-SCR reaction was initiated subsequently by switching the gas mixture to NH_3/NO/O_2 at the same temperature. The reaction temperature was decreased stepwise (50 °C per step) in the range of 500 °C to 100 °C. The gas concentrations after stabilization for at least 0.5 h were used to calculate the conversions at selected temperatures. The sensitivity factors of the analyzed lines were calibrated using commercial mixtures of the gases. The NO conversion in NH_3-SCR was determined based on the following equation (Eq. (2)):

$$X_{NO} = \frac{C_{in,NO} - C_{out,NO}}{C_{in,NO}} \times 100\% \quad (2)$$

where $C_{in,NO}$ is the concentration of NO in inlet gases, $C_{out,NO}$ is the concentration of NO in outlet gases. Apart from N_2, any other N-containing products in NH_3-SCR were detected using QMS analysis.

2.3. In situ IS and IS-DRIFTS measurements

Schematics and instrumental configurations for *in situ* IS and *in situ* IS-DRIFTS are detailed elsewhere [25,33,34]. To achieve a better electrical contact, zeolite powders were deposited as a thick film on an alumina chip with interdigital electrodes (IDEs) on the front side and integrated heater on the back side. *In situ* IS measurements were performed in a stainless-steel measuring chamber (with a total volume of 30 cm^3) equipped with a ZnSe-window for contactless temperature monitoring by a spectral pyrometer (Heitronics), a digital multimeter (Keithley) for the power supply of the integrated heater, and a dosing system for gases related to NH_3-SCR reaction. The measurements were conducted in a broad frequency range of 0.1 Hz to 1 MHz in order to

determine the resonance frequencies of the zeolite catalyst.

For *in situ* IS-DRIFTS, the IDE chip was placed in a home-made reaction chamber with the deposited zeolite film being in the focal point of the infrared beam. DRIFTS measurements were performed using a VERTEX 70 spectrometer (Bruker) in combination with a Praying Mantis (Harrick) mirror system for diffuse reflection spectroscopy. A dome with optical windows was used to cap the reaction chamber, which allows *in situ* measurements under flowing gas conditions. The spectra were recorded in the range from 4000 to 600 cm^{-1} with a resolution of 2 cm^{-1} and each consists of 128 single scans. The IR signals are given in Kubelka-Munk (KM) units to ensure linear correlation between the band intensity and the abundance of surface species. Difference spectra are used to emphasize the vibration modes of the adsorbed species and to exclude lattice vibration of the zeolites. For this purpose, a spectrum of the pure sample at the desired temperature was collected in flowing N_2 as background and was subtracted from all further measurements of the series in differential reaction mixtures. In parallel to DRIFTS, the electrical impedance of the same catalyst film was monitored by means of IS with an impedance analyzer combined with a dielectric interface (both from Solartron). The IS measurements were conducted at a fixed frequency of 10 kHz to achieve high time resolution, and the absolute values of 1/|Z| (*i.e.* admittance) were used for the evaluation of ionic conductivity [17,34,35]. Both IS signal and the DRIFTS signals at characteristic wavenumber were normalized using the respective signal of the NH_3-saturated sample as references. Prior to each IS or IS-DRIFTS measurement, the zeolite samples were held at 450 °C in pure O_2 flow for ca. 1 h to avoid effects of solvent molecules.

2.4. Computation details

Real-space grid-based periodic DFT calculations on the Cu-ZSM-5 and Cu SAPO-34 systems were carried out employing the GPAW electronic structure code [36]. BEEF-vdW functional [37], which is Bayesian error-corrected and is known for better performance as compared to conventional PBE functionals while accounting of van der Waals interactions [38], was used. Although computationally expensive, specifically for molecular adsorption in zeolites, BEEF-vdW has been shown to improve the energetic description systematically among all the DFT-functionals that treat long-range correlations explicitly, and thus brings a clear improvement as compared with the first generation vdW-DF type functionals [30,31]. A grid spacing of 0.18 Å was used where spacing less than 0.2 Å showed no appreciable difference in energies. A Fermi-Dirac smearing width of 0.01 was applied. 2 × 2 × 3 gamma-centered k-points were used for the ZSM-5 supercell of size 20.3686 Å × 20.0117 Å × 13.3242 Å containing 288 atoms, whereas 3 × 3 × 3 gamma-centered k-points were used for the SAPO-34 supercell of size 14.0482 Å × 14.0482 Å × 15.3318 Å containing 108 atoms. The resulting forces in each case were converged to less than 0.05 eV/Å.

For ZSM-5, several (> 50) possible substitution locations of the Al atoms spaced either 1 or 2 Si atoms apart from each other were considered in rings of different sizes, *i.e.* 5MR, 6MR, 7MR, or 10MR. Similarly, all possible locations of the Si atoms were considered in rings of different sizes, *i.e.* 4MR, 6MR, 8MR for SAPO-34. In both cases, the top five most stable locations differed by less than 0.1 eV in energy. Besides, corresponding to any of the reaction steps, five or more different initial configurations and orientations of the reactants were considered for each adsorption case to be able to locate the thermodynamically most stable configuration.

The Gibbs free energy (ΔG) of any reaction was calculated as:

$$\Delta G = \Delta E_{DFT} + \Delta ZPE - T\Delta S \quad (3)$$

wherein ΔZPE refers to the difference in zero-point vibrational energy between the adsorbate-bound site and the bare site, T is the measured temperature (*i.e.* 448 K) and ΔS is the entropy change (assumed to be one third of the gas-phase translational entropy of the adsorbate) [4]. Here, the correction terms (ΔZPE - $T\Delta S$) were applied by considering the reacting species as "mobile", as done in the work of Paolucci et al [3].

Table 1
Physicochemical properties of H- and Cu-ZSM-5 zeolite catalysts.

	Sample	Cu wt%	Cu/Al or Cu/Si ratio	Surface area $m^2\ g^{-1}$)	Pore volume ($cm^3\ g^{-1}$)	Surface Acidity (mmol g^{-1})
1	H-ZSM-5	0	0	336.4	0.12	1.89
2	Cu-ZSM-5	0.64	0.088	334.3	0.12	1.98
3	Cu-ZSM-5	0.99	0.136	322.2	0.12	2.12
4	Cu-ZSM-5	1.17	0.161	306.5	0.11	2.16

Note: Cu loadings (wt%) and Cu/Al (Cu/Si) ratios were determined by ICP-OES. Surface area and pore volume were derived from N_2-physisorption measurements. Surface acidity was obtained from NH_3-TPD.

3. Results and discussion

3.1. Physicochemical properties of Cu-ZSM-5

The H- and Cu-ZSM-5 zeolite catalysts used in this study were examined using ICP-OES, N_2-physisorption and NH_3-TPD, *etc.*, and the derived physicochemical properties are summarized in Table 1. XRD patterns and DR UV/Vis spectra for the synthesized Cu-ZSM-5 catalysts are displayed in Figs. 1 and S1, respectively. Reflections from copper oxides were not detected by XRD for all the three Cu-ZSM-5 samples, indicating the absence of large crystalline domains typically resulting from severe agglomeration of metal species (Fig. 1). DR UV/Vis spectra of the Cu-ZSM-5 zeolites (Fig. S1) show charge transfer (CT) bands mainly below 300 nm, which can be assigned to the $O^{2-} \rightarrow Cu^{2+}$ CT transitions of isolated Cu^{2+} species [32,39–41].

In the NH_3-TPD profiles for Cu-ZSM-5 catalysts (Fig. 2a), three major contributions, namely the desorption peak at ca. 115 °C for weakly adsorbed NH_3 species on Lewis sites (*e.g.* the extra-framework Al sites), the desorption peak at ca. 335 °C for ammonium ion (NH_4^+) species strongly adsorbed on Brønsted sites, and the desorption peak at ca. 230 °C for NH_3 species adsorbed on Cu sites with an intermediate strength [8,25,42], can be resolved. With the increase of Cu exchange level (*i.e.* Cu/Al ratio), an increase of NH_3 desorption from Cu sites as well as a decrease of NH_4^+ desorption from Brønsted sites was observed, due to the fact that Cu^{2+} ions were introduced into the zeolite

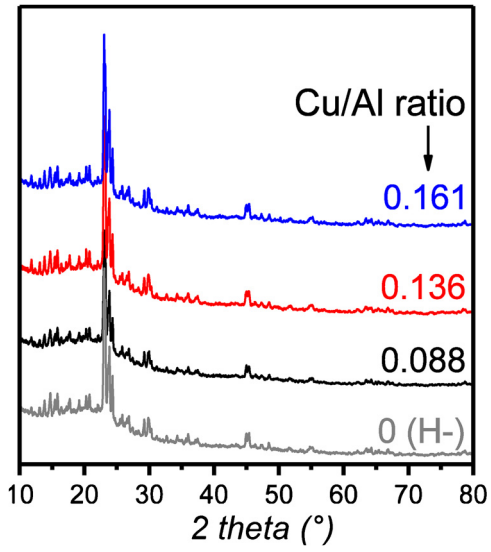

Fig. 1. XRD patterns for the synthesized Cu-ZSM-5 zeolites.

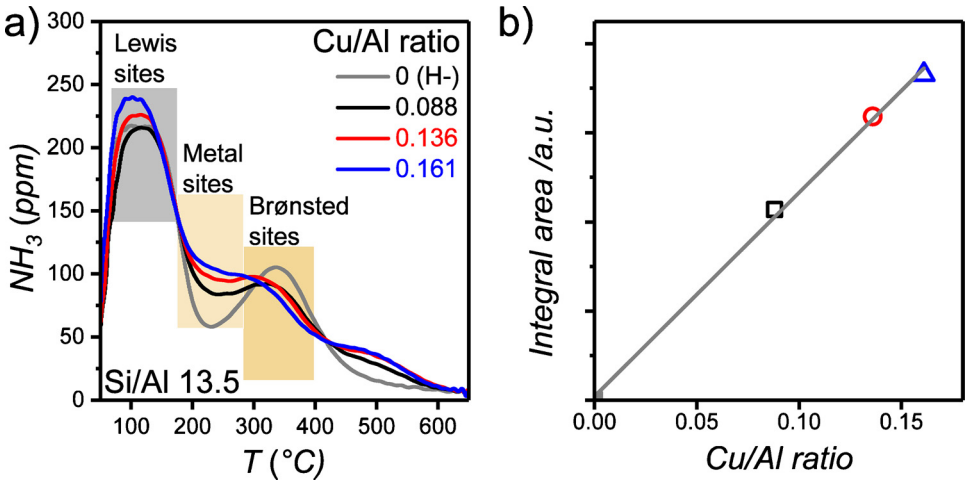

Fig. 2. (a) NH_3-TPD profiles for the H- and Cu-ZSM-5 zeolites; (b) integral peak area for the desorption of NH_3 from Cu sites derived from the deconvolution of the NH_3-TPD profiles in Fig. 2a.

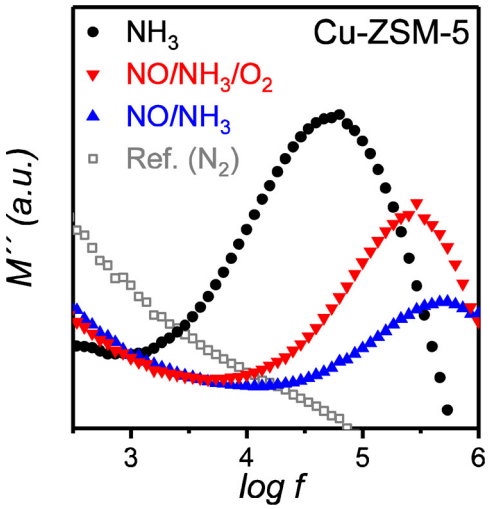

Fig. 3. High-frequency (HF) resonance peaks in the modulus spectra for Cu-ZSM-5 (Si/Al 13.5, Cu/Al 0.136) exposed to different atmospheres at 175 °C. The samples were pretreated at 450 °C in O_2 for 1 h. NH_3: 100 ppm in N_2; NO: 100 ppm in N_2; O_2: 10 vol% in N_2.

via ion exchange with the protons on Brønsted sites [25,43]. Quantitative analysis by peak deconvolution revealed a linear correlation between the integral area for Cu-bounded NH_3 and the Cu/Al ratio (Fig. 2b), indicating a similar interaction between NH_3 and the introduced Cu species in the synthesized Cu-ZSM-5 zeolites with different Cu/Al ratios.

It has to be noted that the local structure of Cu in ZSM-5 is rather complicated, because of the existence of multiple hosting sites for the exchanged Cu ions [7,44] and the formation of oxo-dimeric $[Cu\text{-}O\text{-}Cu]^{2+}$ species at relatively high Cu/Al ratios [14,45,46]. Nevertheless, such site heterogeneity and complexity are not expected to influence significantly the solvation of Cu species by NH_3. On the one hand, the NH_3 solvation effect was found to be insensitive to the zeolite topology and the initial location of the Cu species [9,45]. On the other hand, $[Cu\text{-}O\text{-}Cu]^{2+}$ dimers in Cu-ZSM-5 can be solvated by NH_3 molecules forming isolated Cu-NH_3 species as well [45].

3.2. Modulus spectroscopy study of Cu-ZSM-5

Modulus spectroscopy is known to be highly suitable for resolving multiple (often competing) ion-conducting processes (in particular for determining the dielectric relaxations) that exist in one complex system [47]. As we discriminated previously, the solvation of zeolite with NH_3 led to two different ion movement/conduction processes, namely the long-range transport (across the zeolite lattice) and the short-range or local movement (usually within a constraint space close to the equilibrium site), and consequently increased the ionic conductivity of the zeolite that can be analyzed by *in situ* IS [25,33]. These two ion movement phenomena, occurring at significantly different timescales, induce distinct dielectric relaxation processes which can be visualized by resonance peaks at different frequencies based on

$$f = 1/\tau \quad (4)$$

with f the resonance frequency and τ the related relaxation time in modulus spectra [25,33,47].

To prove the concept of direct monitoring of Cu mobility, we performed detailed *in situ* IS measurements over a selected Cu-ZSM-5 catalyst (Cu/Al 0.136), which was later compared with the commercially relevant Cu-SAPO-34 catalyst (Cu/Si 0.131; see Table S1). In the modulus spectrum collected in NH_3 atmosphere over the Cu-ZSM-5 (Fig. S2a), both low-frequency (LF; below 10 Hz) and high-frequency (HF; 10^4 to 10^6 Hz) peaks, resulting from the long-range (slow) and short-range (fast) ion movement processes [17,25,32,35], respectively, were clearly visible. Interestingly, the HF ion movement, while is determined exclusively by the presence of NH_3 and insensitive to the co-fed NO or NO/O_2 in case of Cu-free H-ZSM-5 (Fig. S2b), is highly sensitive to the co-existence of NO or NO/O_2 with NH_3 in case of Cu-ZSM-5 (Fig. 3). Specifically, the HF resonance peak was shifted remarkably from *log f* 4.80 ($\sim 6.3 \times 10^4$ Hz) in NH_3 to *log f* 5.74 ($\sim 5.5 \times 10^5$ Hz) in $NO/NH_3/O_2$, and to an even higher frequency (*log f* 5.76; $\sim 5.7 \times 10^5$ Hz) in NO/NH_3, corresponding to the shortening of relaxation time for the ion movement, *i.e.* the increasing of ion mobility. It has been predicted theoretically that the Cu mobility is enhanced under NH_3-SCR conditions [2,4]. We therefore attribute the gas condition-dependent HF peak shift in Cu-ZSM-5 (not observed in H-ZSM-5) to the reinforced local movement of the exchanged Cu ions.

As revealed previously, isolated Cu sites in various Cu-zeolites (including Cu-MFI, Cu-CHA, Cu-BEA, *etc.*) can be solvated by NH_3 at low temperatures (below 250 °C) [4,6,18], resulting in mobile Cu species that move rather freely in a constraint volume within the zeolite host (*e.g.* in the cage of CHA-type zeolite) [2,4]. Under similar solvating conditions (*i.e.* non-solvated or NH_3-solvated), the Cu^I species are much more mobile than the Cu^{II} species [4]. While a fraction of Cu^{II} within Cu-zeolites is reduced to Cu^I in $NO/NH_3/O_2$ atmosphere due to the $Cu^{II} \leftrightarrow Cu^I$ redox cycle in standard NH_3-SCR reaction (Eq. (5))

$$4NH_3 + 4NO + O_2 \rightarrow 4N_2 + 6H_2O \quad (5)$$

almost all the reducible Cu^{II} species can be converted to Cu^{I} in NO/NH_3 atmosphere due to the absence of O_2 preventing the $Cu^{I} \rightarrow Cu^{II}$ re-oxidation [4,5]. As a result of the increased Cu^{I} fraction, the local ion conduction in Cu-zeolites was enhanced leading to corresponding shift of the HF peaks toward high frequencies in modulus spectra (Fig. 3). Similar enhanced local ion conduction, indicated by the shift of HF peak, was observed over Cu-ZSM-5 at a higher temperature of 200 °C as well (Fig. S3a). Notably, at 250 °C the HF peak of Cu-ZSM-5 shifted only slightly in NO/NH_3 and negligibly in $NO/NH_3/O_2$ as compared to that in NH_3 (Fig. S3b), which is consistent with the loss of mobile Cu species at such relatively higher temperature as observed previously with *operando* XAS/XES techniques [18,21]. Shift of HF peak was not observed at 200 °C and 250 °C over H-ZSM-5 without Cu ions (Fig. S4).

In addition to NH_3-solvated Cu species, NH_4^+ species may also travel across channels or cages within zeolite frameworks (although a higher energy barrier needs to be overcome) and contribute to the overall local ion conduction [22]. To separate the NH_4^+ contribution, we performed comparative measurements at 175 °C (much lower than the desorption temperature of NH_4^+) by exposing NH_3-saturated Cu-zeolites to N_2 (for desorption of NH_3 from Cu sites) or NO (for reduction of Cu^{II} to Cu^{I}) until steady states. Compared to the counterpart in NH_3, the LF peak of Cu-ZSM-5 kept intact after exposure in either N_2 or NO (in Fig. S5), reflecting similar long-range ion conduction properties in the two experiments. The HF peak of Cu-ZSM-5, however, shifted considerably to lower frequencies after N_2 exposure (Fig. 4), which is attributed to the NH_3 desorption from Cu sites decreasing the Cu mobility, *i.e.* to a weaker NH_3 solvation effect. On the contrary, after NO exposure, the HF peak largely retained in its frequency position or even shifted slightly to higher frequencies (Fig. 4a). While NH_3 desorption from Cu sites and consequently loss of Cu mobility certainly took place during exposure in NO (similar as in N_2), the retaining of local Cu ion movement can be attributed to the formation of more mobile Cu^{I} species resulting from the reduction of Cu^{II} by $NO\text{-}NH_3$ interaction [4,5,32]. As suggested by our previous investigation on the formation of NH_4^+ resulting from the $Cu^{II} \rightarrow Cu^{I}$ reduction, reduction of Cu^{II} in Cu-ZSM-5 can be achieved by such consecutive feeding of NH_3 and NO at 175 °C [32]. Therefore, the HF peak shift of NH_3-loaded Cu-ZSM-5 after NO exposure in comparison with N_2 exposure, *i.e.* $\Delta log\ f_{HF}$ in Fig. 4a, can be adopted to estimate the net contribution of Cu^{I} species to the overall ion conduction. By comparing Cu-ZSM-5 with different Cu/Al ratios (see Table 1), we found the $\Delta log\ f_{HF}$ value at 175 °C increased linearly with Cu/Al ratio (Fig. 4b; related modulus spectra are included Fig. S6), confirming the dependence of local ion movement on the Cu^{I} prosperity in Cu-ZSM-5.

3.3. In situ IS-DRIFTS study of Cu-ZSM-5

The molecular origin of the local Cu ion movement was studied by *in situ* IS-DRIFTS, which allows to monitor simultaneously the surface molecular processes on and ionic conductivity of zeolite catalyst [25,33,34]. The Cu-zeolite catalysts were first exposed to NH_3 until saturation and then to NO or NO/O_2 mixtures for surface reactions, and the DRIFT spectra as well as impedance signal (at a fixed frequency of 10 kHz for a higher time resolution) were collected simultaneously and continuously. In the selected DRIFT spectra in Fig. S7, characteristic bands for NH_3 species on Lewis sites (at 1617 cm^{-1}), NH_4^+ ions on Brønsted acid sites (at 1457 cm^{-1}) and NH_3 species on Cu sites (at 1276 cm^{-1}) were observed (see Table S2 for detailed band assignments) [30,33]. Fig. 5a and b demonstrate the normalized ionic conductivity (I_{IS}) and intensities of the characteristic IR bands (referenced to the respective value after NH_3 saturation) from the IS-DRIFTS measurements over NH_3-saturated Cu-ZSM-5 during exposure in NO/O_2 and NO, respectively. Immediate and rapid consumption of NH_3 on Cu sites (the band at 1276 cm^{-1}; triangles in Fig. 5a) was observed over the Cu-zeolite, consistent with the high reactivity of the species in NH_3-SCR reaction as observed in previous spectroscopic studies [42]. Interestingly, the 1457 cm^{-1} band for NH_4^+ underwent an unexpected further increase in intensity (by ca. 10%) before it decreased slowly to NH_3-free state (Fig. S8 and 5a), demonstrating the formation of NH_4^+ intermediates in the beginning of NO/O_2 exposure [5,17]. Along with the increase of NH_4^+ band, the ionic conductivity of Cu-ZSM-5 increased rapidly as well, pointing to the substantial impact of NH_4^+ intermediates on the ion conduction within the zeolite catalyst [17,35]. Afterwards, the I_{IS} signal of Cu-ZSM-5 decayed slowly following a similar course as for the 1457 cm^{-1} band (Fig. 5a), and both signals reached NH_3-free states simultaneously after ca. 180 min (not shown). When the NH_3-saturated Cu-ZSM-5 was exposed to NO (Fig. 5b), the I_{IS} signal and the 1457 cm^{-1} band increased simultaneously and reached their maxima after ca. 18 min, similar as what observed in the beginning of NO/O_2 exposure (Fig. 5a), and were stabilized afterwards. As disclosed by the LF resonance peaks in Fig. S5, the long-range ion movement in Cu-ZSM-5 kept intact after NO exposure. The increase of ionic conductivity, observed during NO exposure and in the beginning of NO/O_2 exposure, can be thus attributed to the enhanced local movement of Cu ions. In both NO/O_2 and NO atmospheres (Fig. 5a and b), the 1276 cm^{-1} band decreased rapidly along with the increase of the 1457 cm^{-1} band and the I_{IS} signal, suggesting the involvement of Cu-bound NH_3 species in the formation of NH_4^+ intermediates [2,4,5].

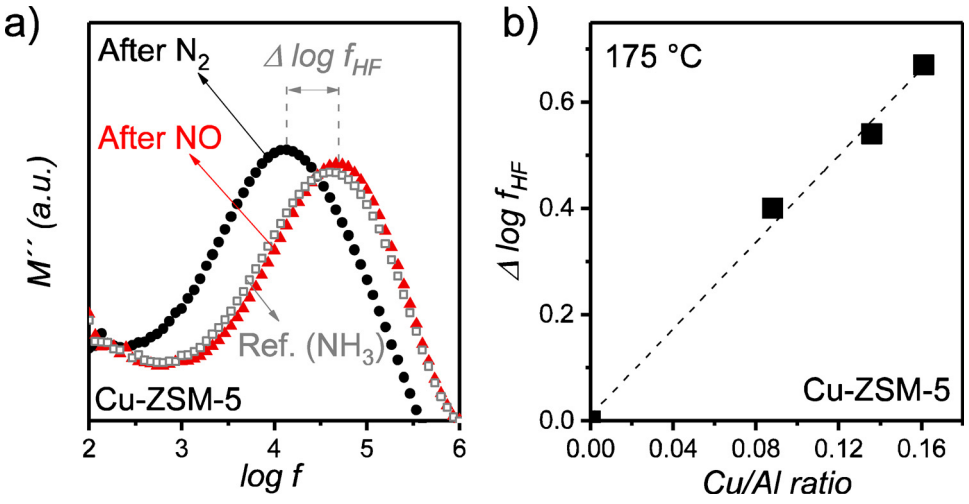

Fig. 4. (a) HF resonance peaks in the modulus spectra for NH_3-saturated Cu-ZSM-5 (Cu/Al 0.136; empty squares) after exposure in N_2 (solid spheres) or NO (solid triangles) to steady states at 175 °C; (b) correlation of $\Delta log\ f_{HF}$ and Cu/Al ratio in Cu-ZSM-5 zeolites at 175 °C. $\Delta log\ f_{HF}$ refers to the HF peak shift of NH_3-loaded Cu-ZSM-5 after NO exposure in comparison with N_2 exposure. Additional modulus spectra for the samples in Fig. 4b are shown in Fig. S9. The samples were pretreated at 450 °C in O_2 for 1 h before each measurement. NH_3: 100 ppm in N_2; NO: 100 ppm in N_2; O_2: 10 vol% in N_2.

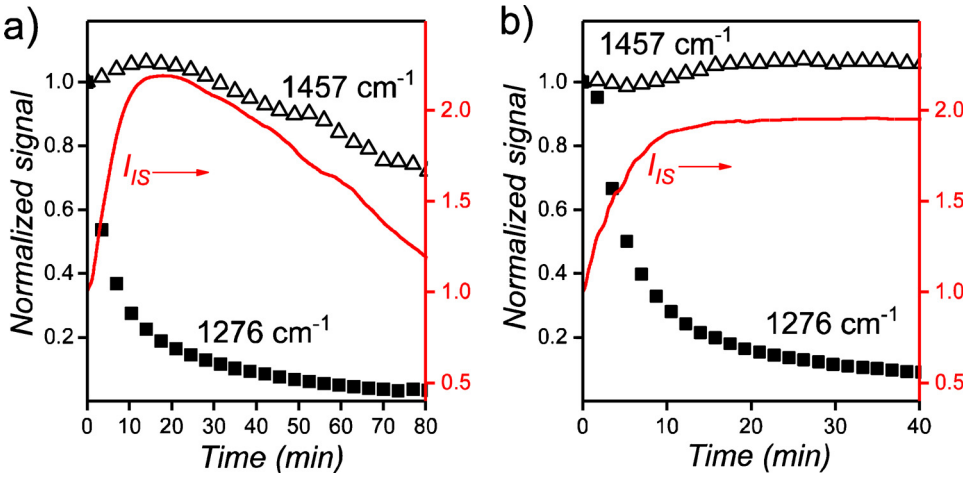

Fig. 5. Normalized ionic conductivity (I_{IS}; red line) and DRIFTS signals (black symbols) at characteristic wavenumbers of NH_3-loaded Cu-ZSM-5 (Cu/Al 0.136) exposed to (a) NO/O_2 or (b) NO mixture. I_{IS}: absolute value of complex admittance $1/|Z|$ at 10 kHz. 1457 cm^{-1}: NH_4^+ ions on Brønsted acid sites; 1276 cm^{-1}: NH_3 species on Cu sites. The respective value after NH_3 saturation was used as reference for normalization. The sample was pretreated at 450 °C in O_2 for 1 h before each measurement. NH_3: 100 ppm in N_2; NO: 100 ppm in N_2; O_2: 10 vol% in N_2.

3.4. Modulus and in situ impedance-DRIFT spectroscopy study of Cu-SAPO-34

To probe the generality and usefulness of the impedance-based approach for detecting local Cu motion within Cu-zeolite catalysts, we further performed modulus spectroscopy and *in situ* IS-DRIFTS studies over Cu-SAPO-34, a commercially relevant NH_3-SCR catalyst for the abatement of automotive NO_x emissions [27–29]. According to the physicochemical properties shown in Table S2, the Cu-SAPO-34 catalyst has similar Cu loading (1.01%) and exchange level (a Cu/Si ratio of 0.131) as the Cu-ZSM-5 catalyst with a Cu/Al ratio of 0.136. Similarly, Cu species in Cu-SAPO-34 are predominantly in isolated states (CT bands mainly at wavelengths below 300 nm in the DR UV/Vis spectrum in Fig. S9a) without traceable aggregation (no CuO_x reflection in the XRD pattern in Fig. S9b) as well. Nevertheless, the presence of a small amount of CuO_x clusters, which are frequently detected even in Cu-SAPO-34 with a very low Cu loading [48,49], cannot be fully excluded.

Fig. 6 displays the modulus spectra collected over Cu-SAPO-34 at 175 °C under the same conditions as the measurements in Fig. 3. As compared to that in NH_3, the HF peak in the modulus spectrum was shifted clearly in $NO/NH_3/O_2$ and more pronouncedly in NO/NH_3, both toward higher frequencies (Fig. 6). Such phenomena are consistent with what observed in case of Cu-ZSM-5 (Fig. 3). The shift of the HF resonance peak to higher frequencies, corresponding to faster ion movement (*i.e.* shorter relaxation time), suggests that the local movement of Cu ions in both Cu-ZSM-5 (Fig. 3) and Cu-SAPO-34 (Fig. 6) was enhanced by the co-existence of NH_3 and NO (with or without O_2), due to the formation of high mobile Cu^I species by Cu^{II} reduction [2,4,5]. Remarkably, for Cu ion motion within Cu-SAPO-34 at 200 °C, the relaxation time 5.4×10^{-6} s, corresponding to a measured resonance frequency of 1.85×10^5 Hz (see the modulus spectrum recorded in NO/NH_3 in Fig. S10), is different from the theoretically predicted value of 1.7×10^{-7} s (corresponding to a hopping rate of 6×10^6 s^{-1}) for the inter-cage diffusion of NH_3-solvated Cu^I species [2]. As we discussed in Section 3.2, in addition to the highly mobile NH_3-solvated Cu^I, less mobile species such as NH_3-solvated Cu^{II} and NH_4^+ also contribute to the overall local ion motion [4,22], and may be largely responsible for the clearly longer relaxation time as inferred from modulus studies. On the other hand, the Cu-SAPO-34 examined here is different from the Cu-SSZ-13 model system used by Paolucci et al. [2] in terms of Si/Al (or [Al + P]/Si) and Cu/Al (or Cu/Si) ratios. Consequently, two key factors determining the motion of NH_3-solavted Cu species, *i.e.* the Cu density and the electrostatic tethering to the framework Al (for Cu-SSZ-13) or Si (for Cu-SAPO-34) centers [2,50], differ significantly in the two catalysts.

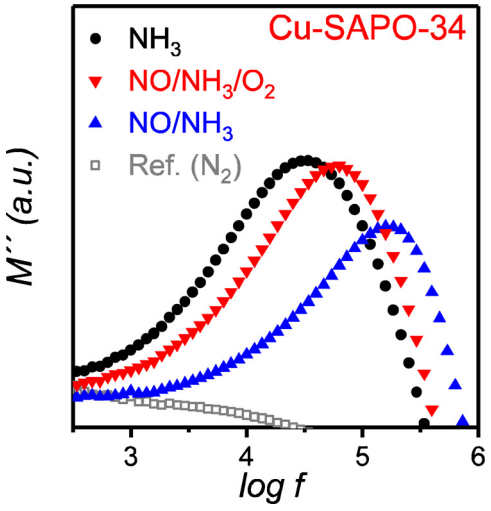

Fig. 6. HF resonance peaks in the modulus spectra for Cu-SAPO-34 ([Al + P]/Si 11.2, Cu/Al 0.131) exposed to different atmospheres at 175 °C. The samples were pretreated at 450 °C in O_2 for 1 h. NH_3: 100 ppm in N_2; NO: 100 ppm in N_2; O_2: 10 vol% in N_2.

In IS-DRIFTS measurements, characteristic bands for NH_4^+ ions on Brønsted acid sites and NH_3 species on Cu sites were observed at 1453 cm^{-1} and 1273 cm^{-1}, respectively, in the DRIFT spectra (Fig. S11) [48,51,52]. Fig. 7a and b demonstrate the normalized ionic conductivity I_{IS} and intensities of the characteristic IR bands (referenced to the respective value after NH_3 saturation) for NH_3-saturated Cu-SAPO-34 during exposure in NO/O_2 and NO, respectively. As shown in Fig. 7a, the ionic conductivity of Cu-SAPO-34 is generally more dependent on the Cu-bound NH_3 species (*i.e.* the 1273 cm^{-1} band), indicating the most influential NH_3 species for the local movement of Cu ions are different for Cu-SAPO-34 and Cu-ZSM-5. Similar as the case of Cu-ZSM-5 (Fig. 5), simultaneous intensity increase of the I_{IS} and the 1453 cm^{-1} band were clearly observed as well in the beginning of NO/O_2 exposure (Fig. 7a), due to the formation of NH_4^+ intermediates promoting the ion conduction in Cu-SAPO-34. Upon exposure in NO (Fig. 7b), the 1453 cm^{-1} band increased and reached its maximum within a short period of ca. 8 min. In this period, a simultaneous increase of I_{IS} was observed as well. Afterwards, while the 1453 cm^{-1} band was maintained at the high level, the I_{IS} signal decreased slowly following a similar trend as the 1273 cm^{-1} band (Fig. 7b). The complicated evolution behavior of I_{IS} in both measurements (Fig. 7a and b) confirms that, despite its dependence on the Cu-bound NH_3 species, the Cu mobility in Cu-SAPO-34 was substantially influenced by the formed NH_4^+ intermediates as well.

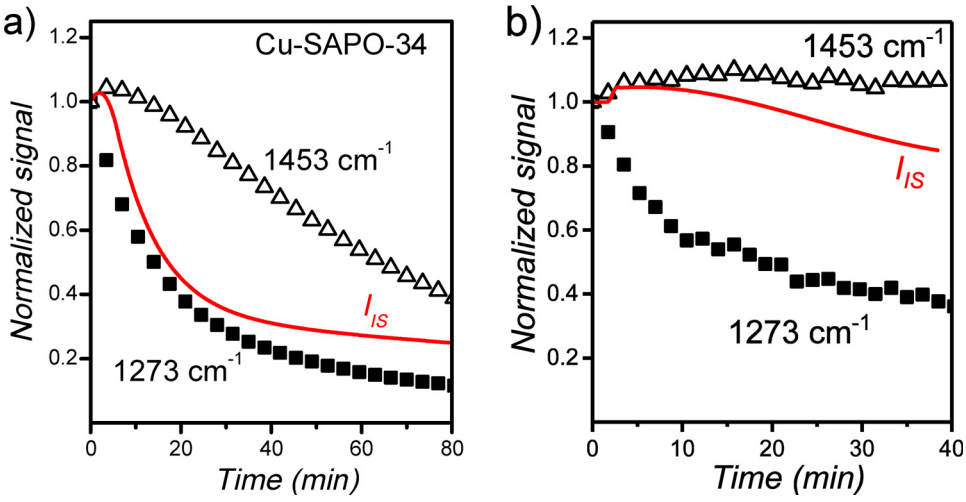

Fig. 7. Normalized ionic conductivity (I_{IS}; red line) and DRIFTS signals (black symbols) at characteristic wavenumbers of NH_3-loaded Cu-SAPO-34 exposed in (a) NO/O_2 or (b) NO mixture. I_{IS}: absolute value of complex admittance $1/|Z|$ at 10 kHz. 1453 cm^{-1}: NH_4^+ ions on Brønsted acid sites; 1273 cm^{-1}: NH_3 species on Cu sites. The sample was pretreated at 450 °C in O_2 for 1 h before each measurement. NH_3: 100 ppm in N_2; NO: 100 ppm in N_2; O_2: 10 vol% in N_2.

3.5. Comparative DFT calculation study of Cu-ZSM-5 and Cu-SAPO-34

DFT calculations were then performed using the BEEF-vdW functional [37] (see sub-section *2.4 Computation details*) for better understanding the observations with respect to the local movement of Cu ions within the two Cu-zeolites. According to literature, in both MFI and CHA frameworks, there are a number of sites being able to host Cu ions [7,8,44]. The NH_3 solvation of Cu species, however, was found to be insensitive to the initial Cu location and even the zeolite topology [4]. Therefore, only the thermodynamically most stable configuration was examined in detail for each zeolite catalyst [5,44]. For ZSM-5, more than 50 possible substitution locations of the Al atoms, spaced either 1 or 2 Si atoms apart from each other, were screened. For SAPO-34, all possible locations of the Si atoms were compared. The optimized Cu-ZSM-5 (Fig. S12a) and Cu-SAPO-34 (Fig. S12b) supercells were established using the thermodynamically most stable ZSM-5 and SAPO-34 configurations, and are in good agreement with literature reports [44,53]. Additional optimized stable configurations are shown in Figs. S13 and S14 for ZSM-5 and SAPO-34, respectively.

Fig. 8 depicts the DFT-computed, optimized local structures of Cu in Cu-ZSM-5 and Cu-SAPO-34. To understand the local movement of Cu ions in NH_3-SCR catalysis, we considered the reaction chemistry and Cu redox cycle as proposed by Paolucci et al. [5], *i.e.* a complete catalytic cycle consists of a $Cu^{II} \rightarrow Cu^{I}$ reduction half-cycle (Eq. (6)) and a $Cu^{I} \rightarrow Cu^{II}$ re-oxidation half-cycle (Eq. (7)).

$$Cu^{II} + NH_3 + NO \rightarrow Cu^{I}/H^+ + H_2O + N_2 \quad (6)$$

$$Cu^{I}/H^+ + NH_3 + NO + 0.5O_2 \rightarrow Cu^{II} + 2H_2O + N_2 \quad (7)$$

While an accurate description of transition states with included ion dynamics is necessary to capture the complete kinetics, DFT simulations can offer a comprehensive description of the thermodynamic landscape which can aid our understanding of certain reaction coordinates, in particular their stability. Fig. 9 demonstrates the local structures of Cu and the Gibbs free energies of the considered reaction steps for standard NH_3-SCR reaction over Cu-ZSM-5 and Cu-SAPO-34. The zero-Kelvin DFT-calculated binding energy values are listed in Table S3 (see *Supplementary Information*) and compared with those in the work of Paolucci et al. [5].

In Cu-ZSM-5, the Cu cation, which is located in the 6MR containing a single Al T-atom and further charge-compensated with another Al T-atom in the proximal 5MR (Figs. 8a and b, and S15) [7,44], was shifted

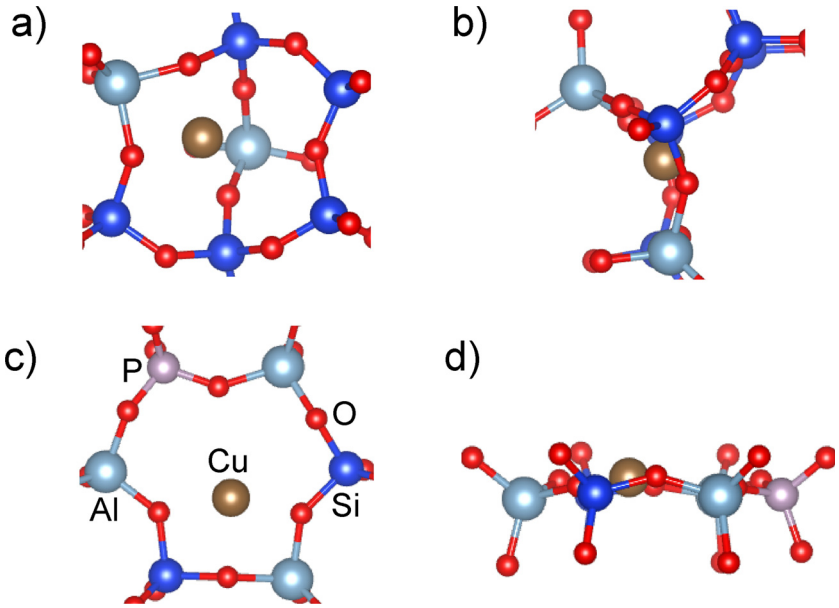

Fig. 8. Top (a and c) and side (b and d) views of the DFT-computed local structures of Cu in ZSM-5 (a and b) and SAPO-34 (c and d). Blue, red, gray, brown and purple spheres indicate Si, O, Al, Cu and P atoms, respectively.

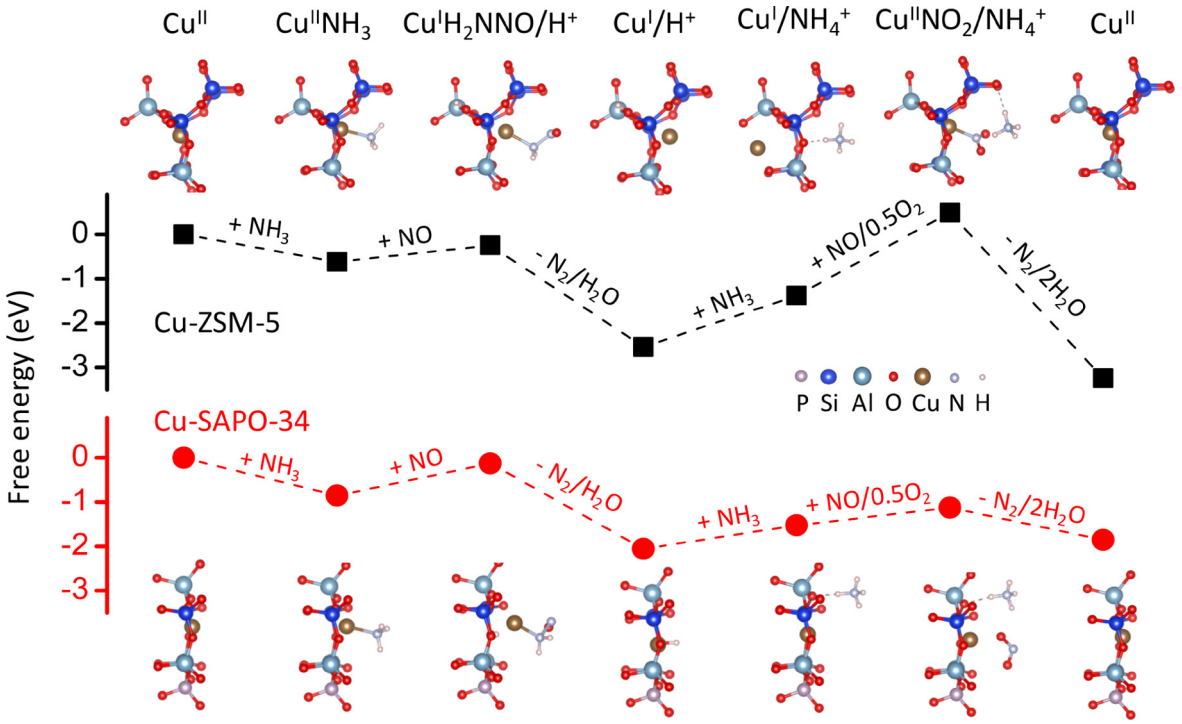

Fig. 9. DFT-computed Cu local structures and free energies along the standard NH_3-SCR reaction pathways over Cu-ZSM-5 (top) and Cu-SAPO-34 (bottom). Blue, red, gray, brown and purple spheres indicate Si, O, Al, Cu and P atoms, respectively.

slightly from its initial siting position (Fig. 9) toward the interconnected 10MR (see Fig. S16 for the extended structures) after binding with a NH_3 molecule ($Cu^{II}NH_3$). The subsequent co-adsorption of NO on $Cu^{II}NH_3$ led to the reduction of Cu^{II} to Cu^{I} and the formation of $Cu^{I}H_2NNO/H^+$ intermediate [2,4,5] with the Cu^{I} locating even closer to the 10MR center. Surprisingly, the Cu^{I}, while largely retained in the position after the release of N_2 and H_2O, was drastically pushed away from the 10MR center after NH_4^+ formation (Figs. 9 and S16), ending up on the very opposite side of the NH_4^+ intermediate. The effect can result from two causes: (1) steric hindrances, which would cost a high energy penalty to fit both of them in a dense pore space, especially in the presence of electrostatic tethering from the Al center in the 5MR [2], and (2) change in the partial charge of the N atom in NH_3 upon protonation, which is expected to result in an electronic repulsion between NH_4^+ and Cu^+. A further binding of Cu^{I}/NH_4^+ with NO/O_2 led to the $Cu^{II}NO_2/NH_4^+$ intermediate with the Cu moving back to the 10MR again. The decomposition of such intermediate to N_2 and H_2O led to Cu^{II} back to its initial position on the zeolite lattice.

Over Cu-SAPO-34, the Cu^{II} siting on the 6MR plane (Fig. 8c and d) was shifted slightly after NH_3 adsorption ($Cu^{II}NH_3$) and more pronouncedly after the subsequent co-adsorption of NO ($Cu^{I}H_2NNO/H^+$), both toward the center of the CHA cage (Fig. 9), and similar to the shift of Cu location in case of Cu-ZSM-5 in the respective reaction coordinate. In stark contrast, the Cu^{I} in Cu-SAPO-34 was not shifted significantly by the formed NH_4^+ intermediate to the opposite side (*i.e.* toward the center of the double 6MR unit), although a slight shift can be noticed by comparing the structures of the bare Cu^{II} and the Cu^{I}/NH_4^+ (Fig. 9). The Cu was lifted slightly out of the 6MR and toward the CHA cage in the reaction coordinate of $Cu^{II}NO_2/NH_4^+$, which resulted from the interaction of NO/O_2 with Cu^{I}/NH_4^+, and went back to its initial position upon $Cu^{II}NO_2/NH_4^+$ decomposition.

As illustrated clearly from the speciation of Cu positioning by DFT calculations (Fig. 9), in NH_3-SCR cycles, the Cu site moves dynamically and reversibly within a constrained volume close to the initial equilibrium position, in agreement with the enhanced Cu local dynamics in both zeolite catalysts as manifested by the modulus spectroscopy studies (Figs. 3 and 6). On a closer look, it can be seen that, for both systems and both kinds of half-cycles (oxidation and reduction), the free energy landscape has similar trajectory of going uphill or downhill (Fig. 9). The formation of $Cu^{II}NO_2/NH_4^+$, which leads to the re-oxidation of $Cu^{I} \rightarrow Cu^{II}$ by NO and O_2 [2,4,5], is thermodynamically less favorable over Cu-ZSM-5 than Cu-SAPO-34, in line with the slower decay of the NH_4^+ band for Cu-ZSM-5 (Fig. 5a) than for Cu-SAPO-34 (Fig. 7a). It's even more remarkable that the intermediate $Cu^{II}NO_2/NH_4^+$ on Cu-ZSM-5 has a calculated free energy even higher than the original reactants, implying that the overall process could be significantly hindered at lower temperatures over the zeolite catalyst. As already proposed in several studies in literature, NH_4^+ species on Brønsted sites adjacent to the Cu sites play important roles in the $Cu^{I} \rightarrow Cu^{II}$ re-oxidation at low temperatures, because they participate in the formation of key intermediates such as $Cu^{II}NO_2(NH_3)_2/NH_4^+$ [4], $Cu^{II}NO_2/NH_4^+$ [5], $Cu^{II}(NH_3)_4$ [21], *etc*. Here, the close coupling of NH_4^+ intermediate and Cu site within Cu-SAPO-34 likely favored NH_4^+ migration from the adjacent Brønsted site to Cu^{I} [51,54], consequently facilitating the $Cu^{I} \rightarrow Cu^{II}$ re-oxidation *via* $Cu^{II}NO_2/NH_4^+$ [5]. Therefore, the NH_3 inhibition effect of $Cu^{I} \rightarrow Cu^{II}$ re-oxidation, as revealed recently by Marberger et al. [21], could be rapidly eased by the formation of closely coupled Cu^{I}-NH_4^+ pair in case of Cu-SAPO-34 (Fig. 7a). On the contrary, when separated far away from each other as the case of Cu-ZSM-5 (Fig. 9), NH_4^+ migration to Cu site and, consequently, the easing of NH_3 inhibition effect of $Cu^{I} \rightarrow Cu^{II}$ re-oxidation are less inclined to occur, leading to slower decaying of both the NH_4^+ and the overall ionic conductivity (Fig. 5a). As a consequence of the thermodynamically more favorable $Cu^{I} \rightarrow Cu^{II}$ re-oxidation, Cu-SAPO-34 displayed a higher NH_3-SCR activity than Cu-ZSM-5 at low temperatures (Fig. S17), which confirms the Cu^{I} re-oxidation as a rate-determining step in NH_3-SCR catalysis [2,21].

It is important to point out here that, for the Cu ligation, we only considered Cu^{II} coordinated with one NH_3, rather than the fully coordinated tetra-fold $Cu^{II}(NH_3)_4$, in order to understand the effect of accurate van der Waals corrections on the energetics calculation of zeolite systems [30,31]. For further investigations, advanced non-

equilibrium AIMD or metadynamics simulations, as explored recently by different groups [2,6,55,56], are needed to understand more explicitly the kinetic barriers for the local motion of fully NH_3-coordinated and -solvated Cu species (*i.e.* $Cu^{II}[NH_3]_4$ and $Cu^{I}[NH_3]_2$) as well as the key elementary reaction steps (*e.g.* $NO + 0.5O_2 \rightarrow NO_2$).

4. Conclusions

In summary, we show here that complex impedance-based modulus spectroscopy enables direct probing of the dynamic local movement of NH_3-solvated Cu ions in Cu-zeolite catalysts under SCR-related reaction conditions. Gas condition-dependent Cu mobility was confirmed by the resonance frequency shift of the corresponding relaxation process associated with Cu ion movement within zeolite framework structures. The co-adsorption and interaction of NO and NH_3 on Cu^{II} sites led to the formation of highly mobile Cu^{I} species and NH_4^+ intermediates, and, consequently, significantly enhanced local dynamics of Cu ions in both zeolite catalysts. The rate-determining re-oxidation of Cu^{I} was more favorable in Cu-SAPO-34 than in Cu-ZSM-5, which can be attributed to the close coupling of NH_4^+ intermediate and Cu site promoting the formation of Cu^{II}-NO_2/NH_4^+. As a result, the overall local dynamics of Cu, largely determined by Cu^{I} species, is less dependent on the NH_4^+ intermediate in Cu-SAPO-34 than in Cu-ZSM-5. Our study indicates that complex impedance-based modulus spectroscopy is a versatile method for studying the Cu ion movement, and may provide unique insights for understanding the dynamics of isolated metal active sites within zeolite catalysts and single-site catalysts for redox reactions in general.

Acknowledgments

This work was supported by the German Research Foundation (DFG) under grant SI 609/14-1, the Federal Ministry of Education and Research (BMBF) in the context of the DeNOx project (13XP5042A), and the Exploratory Research Space of RWTH Aachen University financed by the Excellence Initiative of the German federal and state governments to promote science and research at German universities. P. C. appreciates the funding from the Xinghua talent program of South China University of Technology. We thank Dr. D. Rauch and Prof. R. Moos for fruitful discussions and for providing IDE chips, and Dr. P. Weide and Dr. P. Kangvansura for experimental support.

Appendix A. Supplementary data

Supplementary material related to this article can be found, in the online version, at doi:https://doi.org/10.1016/j.apcatb.2018.05.091.

References

[1] J.H. Kwak, R.G. Tonkyn, D.H. Kim, J. Szanyi, C.H.F. Peden, Excellent activity and selectivity of Cu-SSZ-13 in the selective catalytic reduction of NO_x with NH_3, J. Catal. 275 (2010) 187–190.
[2] C. Paolucci, I. Khurana, A.A. Parekh, S. Li, A.J. Shih, H. Li, J.R. Di Iorio, J.D. Albarracin-Caballero, A. Yezerets, J.T. Miller, W.N. Delgass, F.H. Ribeiro, W.F. Schneider, R. Gounder, Dynamic multinuclear sites formed by mobilized copper ions in NO_x selective catalytic reduction, Science 357 (2017) 898–903.
[3] C. Paolucci, A.A. Parekh, I. Khurana, J.R. Di Iorio, H. Li, J.D. Albarracin Caballero, A.J. Shih, T. Anggara, W.N. Delgass, J.T. Miller, F.H. Ribeiro, R. Gounder, W.F. Schneider, Catalysis in a cage: condition-dependent speciation and dynamics of exchanged Cu cations in SSZ-13 zeolites, J. Am. Chem. Soc. 138 (2016) 6028–6048.
[4] C. Paolucci, A.A. Verma, S.A. Bates, V.F. Kispersky, J.T. Miller, R. Gounder, W.N. Delgass, F.H. Ribeiro, W.F. Schneider, Isolation of the copper redox steps in the standard selective catalytic reduction on Cu-SSZ-13, Angew. Chem. Int. Ed. 53 (2014) 11828–11833.
[5] F. Gao, D. Mei, Y. Wang, J. Szanyi, C.H.F. Peden, Selective catalytic reduction over Cu/SSZ-13: linking homo- and heterogeneous catalysis, J. Am. Chem. Soc. 139 (2017) 4935–4942.
[6] U. Deka, I. Lezcano-Gonzalez, B.M. Weckhuysen, A.M. Beale, Local environment and nature of Cu active sites in zeolite-based catalysts for the selective catalytic reduction of NO_x, ACS Catal. 3 (2013) 413–427.
[7] A.M. Beale, F. Gao, I. Lezcano-Gonzalez, C.H.F. Peden, J. Szanyi, Recent advances in automotive catalysis for NO_x emission control by small-pore microporous materials, Chem. Soc. Rev. 44 (2015) 7371–7405.
[8] C. Paolucci, J.R. Di Iorio, F.H. Ribeiro, R. Gounder, W.F. Schneider, Catalysis science of NO_x selective catalytic reduction with ammonia over Cu-SSZ-13 and Cu-SAPO-34, Adv. Catal. 59 (2016) 1–107.
[9] N. Martín, C. Paris, P.N.R. Vennestrøm, J.R. Thøgersen, M. Moliner, A. Corma, Cage-based small-pore catalysts for NH_3-SCR prepared by combining bulky organic structure directing agents with modified zeolites as reagents, Appl. Catal. B Environ. 217 (2017) 125–136.
[10] U. De-La-Torre, B. Pereda-Ayo, M. Moliner, J.R. González-Velasco, A. Corma, Cu-zeolite catalysts for NO_x removal by selective catalytic reduction with NH_3 and coupled to NO storage/reduction monolith in diesel engine exhaust aftertreatment systems, Appl. Catal. B Environ. 187 (2016) 419–427.
[11] T. Günter, J. Pesek, K. Schäfer, A. Bertótiné Abai, M. Casapu, O. Deutschmann, J.D. Grunwaldt, Cu-SSZ-13 as pre-turbine NO_x-removal-catalyst: impact of pressure and catalyst poisons, Appl. Catal. B Environ. 198 (2016) 548–557.
[12] V.L. Sushkevich, D. Palagin, M. Ranocchiari, J.A. van Bokhoven, Selective anaerobic oxidation of methane enables direct synthesis of methanol, Science 356 (2017) 523–527.
[13] B.E.R. Snyder, P. Vanelderen, M.L. Bols, S.D. Hallaert, L.H. Böttger, L. Ungur, K. Pierloot, R.A. Schoonheydt, B.F. Sels, E.I. Solomon, The active site of low-temperature methane hydroxylation in iron-containing zeolites, Nature 536 (2016) 317–321.
[14] S. Grundner, M.A.C. Markovits, G. Li, M. Tromp, E.A. Pidko, E.J.M. Hensen, A. Jentys, M. Sanchez-Sanchez, J.A. Lercher, Single-site trinuclear copper oxygen clusters in mordenite for selective conversion of methane to methanol, Nat. Commun. 6 (2015) 7546.
[15] L. Shao, B. Zhang, W. Zhang, S.Y. Hong, R. Schlögl, D.S. Su, The role of palladium dynamics in the surface catalysis of coupling reactions, Angew. Chem. Int. Ed. 52 (2013) 2114–2117.
[16] P. Chen, A. Khetan, F. Yang, V. Migunov, P. Weide, S.P. Stuermer, P. Guo, K. Kaehler, W. Xia, J. Mayer, H. Pitsch, U. Simon, M. Muhler, Experimental and theoretical understanding of nitrogen-doping-induced strong metal-support interactions in Pd/TiO_2 catalysts for nitrobenzene hydrogenation, ACS Catal. 7 (2017) 1197–1206.
[17] P. Chen, M. Jabłońska, P. Weide, T. Caumanns, T. Weirich, M. Muhler, R. Moos, R. Palkovits, U. Simon, Formation and effect of NH_4^+ intermediates in NH_3–SCR over Fe-ZSM-5 zeolite catalysts, ACS Catal. 6 (2016) 7696–7700.
[18] K.A. Lomachenko, E. Borfecchia, C. Negri, G. Berlier, C. Lamberti, P. Beato, H. Falsig, S. Bordiga, The Cu-CHA deNO_x catalyst in action: temperature-dependent NH_3-assisted selective catalytic reduction monitored by operando XAS and XES, J. Am. Chem. Soc. 138 (2016) 12025–12028.
[19] M. Moreno-González, B. Hueso, M. Boronat, T. Blasco, A. Corma, Ammonia-containing species formed in Cu-chabazite as per in situ EPR, solid-state NMR, and DFT calculations, J. Phys. Chem. Lett. 6 (2015) 1011–1017.
[20] F. Gao, J.H. Kwak, J. Szanyi, C.H.F. Peden, Current understanding of Cu-exchanged chabazite molecular sieves for use as commercial diesel engine deNO_x catalysts, Top. Catal. 56 (2013) 1441–1459.
[21] A. Marberger, A.W. Petrov, P. Steiger, M. Elsener, O. Kröcher, M. Nachtegaal, D. Ferri, Time-resolved copper speciation during selective catalytic reduction of NO on Cu-SSZ-13, Nat. Catal. 1 (2018) 221–227.
[22] L. Chen, J. Jansson, M. Skoglundh, H. Grönbeck, Mechanism for solid-state ion exchange of Cu^+ into zeolites, J. Phys. Chem. C 120 (2016) 29182–29189.
[23] U. Simon, U. Flesch, Cation-cation interaction in dehydrated zeolites X and Y monitored by modulus spectroscopy, J. Porous Mater. 6 (1999) 33–40.
[24] T. Ohgushi, K. Ishimaru, Y. Adachi, Movements and hydration of potassium ion in K-A zeolite, J. Phys. Chem. C 113 (2009) 2468–2474.
[25] P. Chen, U. Simon, In situ spectroscopic studies of proton transport in zeolite catalysts for NH_3-SCR, Catalysts 6 (2016) 204.
[26] Y. Zheng, Y. Liu, M.P. Harold, D. Luss, LNT-SCR dual-layer catalysts optimized for lean NO_x reduction by H_2 and CO, Appl. Catal. B Environ. 148–149 (2014) 311–321.
[27] K. Leistner, L. Olsson, Deactivation of Cu/SAPO-34 during low-temperature NH_3-SCR, Appl. Catal. B Environ. 165 (2015) 192–199.
[28] K. Leistner, O. Mihai, K. Wijayanti, A. Kumar, K. Kamasamudram, N.W. Currier, A. Yezerets, L. Olsson, Comparison of Cu/BEA, Cu/SSZ-13 and Cu/SAPO-34 for ammonia-SCR reactions, Catal. Today 258 (2015) 49–55.
[29] J. Wang, H. Zhao, G. Haller, Y. Li, Recent advances in the selective catalytic reduction of NO_x with NH_3 on Cu-chabazite catalysts, Appl. Catal. B Environ. 202 (2017) 346–354.
[30] F. Göltl, P. Sautet, Modeling the adsorption of short alkanes in the zeolite SSZ-13 using “van der Waals” DFT exchange correlation functionals: understanding the advantages and limitations of such functionals, J. Chem. Phys. 140 (2014) 154105.
[31] R.Y. Brogaard, P.G. Moses, J.K. Nørskov, Modeling van der Waals interactions in zeolites with periodic DFT: physisorption of n-alkanes in ZSM-22, Catal. Lett. 142 (2012) 1057–1060.
[32] P. Chen, D. Rauch, P. Weide, S. Schönebaum, T. Simons, M. Muhler, R. Moos, U. Simon, The effect of Cu and Fe cations on NH_3-supported proton transport in deNO_x-SCR zeolite catalysts, Catal. Sci. Technol. 6 (2016) 3362–3366.
[33] P. Chen, S. Schoenebaum, T. Simons, D. Rauch, M. Dietrich, R. Moos, U. Simon, Correlating the integral sensing properties of zeolites with molecular processes by combining broadband impedance and DRIFT spectroscopy-a new approach for bridging the scales, Sensors 15 (2015) 28915–28941.
[34] T. Simons, P. Chen, D. Rauch, R. Moos, U. Simon, Sensing catalytic conversion: simultaneous DRIFT and impedance spectroscopy for in situ monitoring of NH_3-SCR on zeolites, Sens. Actuators B Chem. 224 (2016) 492–499.

[35] P. Chen, J. Simboeck, S. Schoenebaum, D. Rauch, T. Simons, R. Palkovits, R. Moos, U. Simon, Monitoring NH_3 storage and conversion in Cu-ZSM-5 and Cu-SAPO-34 catalysts for NH_3-SCR by simultaneous impedance and DRIFT spectroscopy, Sens. Actuators B Chem. 236 (2016) 1075–1082.
[36] J. Enkovaara, C. Rostgaard, J.J. Mortensen, J. Chen, M. Dułak, L. Ferrighi, J. Gavnholt, C. Glinsvad, V. Haikola, H.A. Hansen, H.H. Kristoffersen, M. Kuisma, A.H. Larsen, L. Lehtovaara, M. Ljungberg, O. Lopez-Acevedo, P.G. Moses, J. Ojanen, T. Olsen, V. Petzold, N.A. Romero, J. Stausholm-Møller, M. Strange, G.A. Tritsaris, M. Vanin, M. Walter, B. Hammer, H. Häkkinen, G.K.H. Madsen, R.M. Nieminen, J.K. Nørskov, M. Puska, T.T. Rantala, J. Schiøtz, K.S. Thygesen, K.W. Jacobsen, Electronic structure calculations with GPAW: a real-space implementation of the projector augmented-wave method, J. Phys. Condens. Matter. 22 (2010) 253202.
[37] J. Wellendorff, K.T. Lundgaard, A. Møgelhøj, V. Petzold, D.D. Landis, J.K. Nørskov, T. Bligaard, K.W. Jacobsen, Density functionals for surface science: exchange-correlation model development with Bayesian error estimation, Phys. Rev. B 85 (2012) 235149.
[38] A.J.R. Hensley, K. Ghale, C. Rieg, T. Dang, E. Anderst, F. Studt, C.T. Campbell, J.S. McEwen, Y. Xu, DFT-based method for more accurate adsorption energies: an adaptive sum of energies from RPBE and vdW density functionals, J. Phys. Chem. C 121 (2017).
[39] Y. Li, J. Deng, W. Song, J. Liu, Z. Zhao, M. Gao, Y. Wei, L. Zhao, Nature of Cu species in Cu-SAPO-18 catalyst for NH_3-SCR: combination of experiments and DFT calculations, J. Phys. Chem. C 120 (2016) 14669–14680.
[40] J. Janas, J. Gurgul, R.P. Socha, S. Dzwigaj, Effect of Cu content on the catalytic activity of CuSiBEA zeolite in the SCR of NO by ethanol: nature of the copper species, Appl. Catal. B Environ. 91 (2009) 217–224.
[41] P. Chen, R. Moos, U. Simon, Metal loading affects the proton transport properties and the reaction monitoring performance of Fe-ZSM-5 and Cu-ZSM-5 in NH_3-SCR, J. Phys. Chem. C 120 (2016) 25361–25370.
[42] I. Lezcano-Gonzalez, U. Deka, B. Arstad, A. Van Yperen-De Deyne, K. Hemelsoet, M. Waroquier, V. Van Speybroeck, B.M. Weckhuysen, A.M. Beale, Determining the storage, availability and reactivity of NH_3 within Cu-chabazite-based ammonia selective catalytic reduction systems, Phys. Chem. Chem. Phys. 16 (2014) 1639–1650.
[43] S. Brandenberger, O. Kröcher, A. Wokaun, A. Tissler, R. Althoff, The role of Brønsted acidity in the selective catalytic reduction of NO with ammonia over Fe-ZSM-5, J. Catal. 268 (2009) 297–306.
[44] M.H. Groothaert, K. Pierloot, A. Delabie, R.A. Schoonheydt, Identification of Cu(II) coordination structures in Cu-ZSM-5 based on a DFT/ab initio assignment of the EPR spectra, Phys. Chem. Chem. Phys. 5 (2003) 2135–2144.
[45] F. Giordanino, P.N.R. Vennestrøm, L.F. Lundegaard, F.N. Stappen, S. Mossin, P. Beato, S. Bordiga, C. Lamberti, Characterization of Cu-exchanged SSZ-13: a comparative FTIR, UV–Vis, and EPR study with Cu-ZSM-5 and Cu-β with similar Si/Al and Cu/Al ratios, Dalt. Trans. 42 (2013) 12741–12761.
[46] J.S. Woertink, P.J. Smeets, M.H. Groothaert, M.A. Vance, B.F. Sels, R.A. Schoonheydt, E.I. Solomon, A $[Cu_2O]^{2+}$ core in Cu-ZSM-5, the active site in the oxidation of methane to methanol, Proc. Natl. Acad. Sci. 106 (2009) 18908–18913.
[47] V.F. Lvovich, Impedance Spectroscopy, John Wiley & Sons, Inc., Hoboken, NJ, USA, 2012.
[48] L. Wang, W. Li, G. Qi, D. Weng, Location and nature of Cu species in Cu/SAPO-34 for selective catalytic reduction of NO with NH_3, J. Catal. 289 (2012) 21–29.
[49] F. Gao, E.D. Walter, N.M. Washton, J. Szanyi, C.H.F. Peden, Synthesis and evaluation of Cu-SAPO-34 catalysts for ammonia selective catalytic reduction. 1. Aqueous solution ion exchange, ACS Catal. 3 (2013) 2083–2093.
[50] V. Rizzotto, P. Chen, U. Simon, Mobility of NH_3-solvated Cu^{II} ions in Cu-SSZ-13 and Cu-ZSM-5 NH_3-SCR catalysts: a comparative impedance spectroscopy study, Catalysts 8 (2018) 162.
[51] D. Wang, L. Zhang, K. Kamasamudram, W.S. Epling, In situ-DRIFTS study of selective catalytic reduction of NO_x by NH_3 over Cu-exchanged SAPO-34, ACS Catal. 3 (2013) 871–881.
[52] L. Ma, Y. Cheng, G. Cavataio, R.W. McCabe, L. Fu, J. Li, In situ DRIFTS and temperature-programmed technology study on NH_3-SCR of NO_x over Cu-SSZ-13 and Cu-SAPO-34 catalysts, Appl. Catal. B Environ. 156–157 (2014) 428–437.
[53] Y. Mao, Z. Wang, H.-F. Wang, P. Hu, Understanding catalytic reactions over zeolites: a density functional theory study of selective catalytic reduction of NO_x by NH_3 over Cu-SAPO-34, ACS Catal. 6 (2016) 7882–7891.
[54] Y. Duan, J. Wang, T. Yu, M. Shen, J. Wang, The role and activity of various adsorbed ammonia species on Cu/SAPO-34 catalyst during passive-SCR process, RSC Adv. 5 (2015) 14103–14113.
[55] S. Li, Y. Zheng, F. Gao, J. Szanyi, W.F. Schneider, Experimental and computational interrogation of fast SCR mechanism and active sites on H-form SSZ-13, ACS Catal. (2017) 5087–5096.
[56] H. Li, C. Paolucci, W.F. Schneider, Zeolite adsorption free energies from ab initio potentials of mean force, J. Chem. Theory Comput. 14 (2018) 929–938.